

Phase Locking in Nonlinear Optical Patterns

E. Pampaloni, S. Residori, S. Soria,* and F. T. Arecchi†

Istituto Nazionale di Ottica, 50125 Firenze, Italy

(Received 30 May 1996)

We report a new type of optical patterns induced by phase locking of several wave vectors with different lengths and orientations. Wave vector selection is due to the optical nonlinearity provided by a Kerr-like medium. The system displays pattern multistability. We characterize the different configurations by the distribution of wave vector families in Fourier space. Even close to threshold, the strong coupling among families yields a collective behavior without critical slowing down, at variance with the isolated behavior of each separate family. [S0031-9007(97)02327-2]

PACS numbers: 42.65.Sf, 42.65.Pc, 42.79.Kr

Optical pattern formation emerges from the interaction of nonlinearities and symmetry constraints in spatially extended systems [1]. It shows strong analogies with other areas such as fluid dynamics, chemistry, and biology [2]. In particular, optics provides easily two-dimensional patterns which arise from phase modulation of the transverse profile of an optical beam as it passes through a nonlinear medium [3]. Roll-hexagon transition [4], crystals and quasicrystals [5], and domain coexistence of patterns with different wavelengths [6] have been reported for a system based on a liquid-crystal-light-valve (LCLV) with a nonlocal feedback [7]. The LCLV Kerr-like nonlinearity converts an amplitude into a phase modulation, whereas diffraction due to free propagation converts a phase into an amplitude modulation, so that a positive feedback is realized for all those spatial frequencies satisfying the resonance conditions $q^2 L/2k = \pi/2, 3\pi/2, \dots$, q being the field transverse wave number, $k = 2\pi/\lambda$ the optical wave number, and L the free propagation length. The feedback loop includes a fiber bundle by which the image on the back of the LCLV is rotated by an angle $\Delta = 2\pi/N$ with respect to the front image. This rotation maps a transverse wave vector \vec{q}' into the next one \vec{q}'' with $|\vec{q}'| = |\vec{q}''|$ and their directions rotated by an angle Δ . This way, an N -gonal symmetry is imposed upon the pattern.

The marginal stability curves yielding the threshold input intensity I_{th} vs q^2 consist of a series of convex curves whose minima are aligned along a straight line corresponding to the diffusion loss within the optical medium. This line has a slope proportional to $\sigma^{-1} = l_D^2/\lambda L$ where l_D is the diffusion length of the nonlinear medium [3]. The minima are located at $q_j = \sqrt{2j + 1}q_0$, $q_0 = (2\pi^2/\lambda L)^{1/2}$ being the basic wave number, and $j = 0, 1, 2, 3, \dots$ being the ring order [5]. Within an allowed j ring, the rotation lowers the cylindrical symmetry so that a discrete family of N wave vectors equispaced in angle get excited on that ring. This family yields in real space a 2D tiling consisting of N -gons.

Excitation of a single family is obtained either by adjusting the input intensity close to threshold or by inserting a suitable filter [5]. For higher intensities and

N odd, excitation of two bands yields complex patterns, with many families of wave vectors unrelated in phase, so that the real space tiling consists of many domains [6].

In this Letter we report evidence of a new type of pattern consisting of a single domain, even though its Fourier spectrum contains many families of wave vectors. We show that this can be realized only by mutually phase locking all the different wave vectors. In particular, choosing $N = 6$ and switching on the input intensity from zero, only three combinations of wave vectors provide stable patterns, after a transient in which all families compatible with the symmetry requirements compete.

Experimentally, besides using $N = 6$, we expand and filter the input He-Ne laser beam in such a way that the LCLV is uniformly illuminated over a central region of 1 cm diameter. The free propagation length is fixed to 20 cm; thus $\sigma \approx 2.5 \times 10^2$ and many wave vectors associated with successive minima are simultaneously excited even close to the threshold value $I_{th} = 45.3 \mu\text{W}/\text{cm}^2$. We call $\varepsilon = (I_0 - I_{th})/I_{th}$ the normalized control parameter. For $\varepsilon < 0.05$, the sensitivity of the detection apparatus is too poor to detect a meaningful image. At $\varepsilon = 0.05$ already several rings ($j = 0$ to 5) are above threshold. The actual excitation depends upon the phase relations as discussed below.

The set of three stable patterns is recorded in Fig. 1 for $\varepsilon = 0.2$. By inspection of the Fourier space we see that the power spectrum of the three patterns consists of 4, 4, and 6 families, respectively. We name the families by their ring number, adding an apex whenever there is a degeneracy, as follows: P1: 1, 2, 2', 3; P2: 1, 1', 3, 5; P3: 2, 2', 3, 3', 4, 4'. Notice that the nonlinearities shift the Fourier spots away from the band minima predicted by the linear stability analysis. For example, in the case of P1, $q_1/q_2 \approx 0.76$ instead of $\sqrt{3/5}$ and $q_3/q_2 \approx 1.24$ instead of $\sqrt{7/5}$. Furthermore, the nonlinear coupling partly suppresses the $j = 0$ vector which is rather dim and shifted from $q_0/q_2 = \sqrt{1/3}$ to $q_0/q_2 \approx 0.25$.

Of course, inspection of the power spectrum yields only the relative orientations, but provides no phase information on the amplitude of each wave vector. As

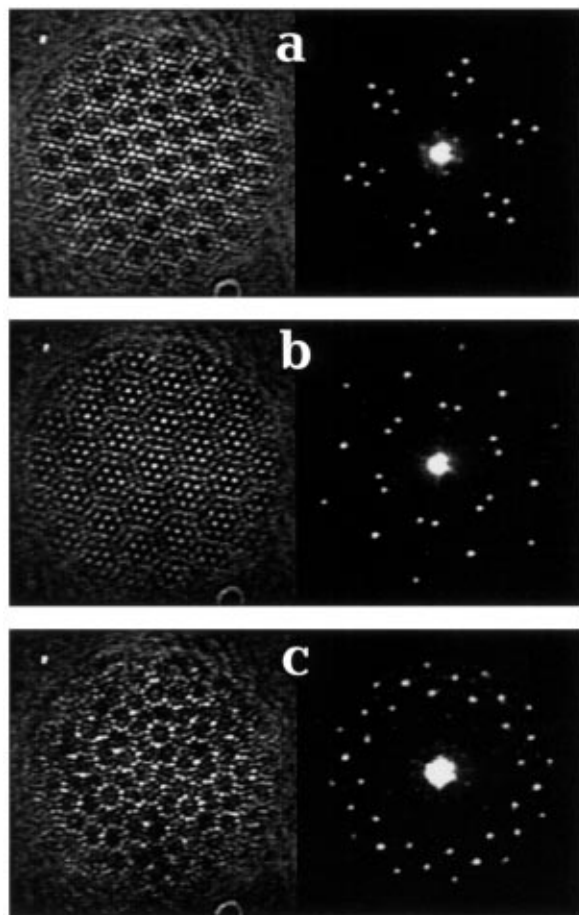


FIG. 1. Near-field (left) and far-field (right) images of the frequency locked patterns: (a) P1, (b) P2, and (c) P3. Near-field images are the intensity distribution on the back plane of the LCLV, whereas far-field images are the corresponding spatial power spectra.

we switch on and off the input intensity leaving an off interval sufficiently long (more than 20 sec) to cancel memory of the previous pattern, the three patterns of Fig. 1 appear with relative frequencies P1: 0.6, P2: 0.25, and P3: 0.15.

For $\varepsilon = 0.2$ the three patterns are stable and robust against external perturbations. However, as ε increases to 0.4, P3 shows fluctuations, and it decays toward P1 and P2 with a lifetime of 50 sec. Eventually for $\varepsilon > 1.2$ the patterns show space-time chaos [8]; indeed they appear as formed of many uncorrelated domains and correspondingly the spectrum is made of continuous rings with no orientation selection. Besides the fixed orientations displayed in Fig. 1, the phases of the wave vectors also bear fixed relations, and hence the observed single domain patterns are a case of phase locking.

We construct geometrically the mutual couplings of the wave vectors involved in the three patterns (Fig. 2). Each j ring is characterized by the summation rule that gives rise to the hexagonal symmetry, i.e., $\vec{q}_j' + \vec{q}_j'' =$

\vec{q}_j , where \vec{q}_j is a vector forming an angle $\Delta = 2\pi/6$ with respect to \vec{q}_j' and \vec{q}_j'' . These intraring couplings correspond to the usual quadratic terms imposed by the medium nonlinearity when only one wave number is excited [4],[9].

More fundamental for the phase locking are the extra-ring couplings, i.e., those ones providing a closure relationship over different j rings. For example, for pattern P1 contributions to rings 1 and 3 come from the sums of two \vec{q}_2 wave vectors. Moreover, ring 2 gives rise to an inner ring 0 which participates to other extra-ring couplings giving contributions to q_1 , q_2 , and q_3 . In summary, denoting each parallelogram by the three component vectors, P1 is made of the following extra-ring couplings: $(1,2,2')$, $(2,2',3)$, $(0,2,2')$, $(0,2,3)$, $(0,2',3)$, $(0,1,2)$, and $(0,1,2')$. Five of these seven parallelograms are shown in Fig. 2 (upper). Similarly the other two patterns include the following extra-ring couplings: $(1,1',3)$, $(1,1',5)$, $(1,3,5)$, and $(1',3,5)$ for P2; $(2,3,4)$, $(2',3,4)$, $(2,3',4)$, and $(2,3,4')$ for P3.

These geometric relations lead to stable patterns only if the corresponding amplitudes are locked in phase. Indeed in the lower part of Fig. 2 we report the near-field patterns obtained by Fourier transformation of the wave vectors shown in the upper part with the phases indicated in the caption, which are 0 for odd rings and $\pm\pi/2$ for even rings. Indeed, it is known that with a defocusing Kerr medium as is our system [4–6] and in the absence of rotation only odd rings ($j = 1, 3, \dots$) are allowed [9]; in the presence of a π rotation ($N = 2$), the even rings are also allowed but wave vectors pair with $\pm\pi/2$ phases [4], [10]. Generalizing to $N > 2$ even, we have families of $N/2$ pairs with $\pm\pi/2$ phases. Besides this dynamical argument, we verify by inspection that any other choice of phases leads to unobserved patterns. The above considerations, together with the fact that the near-field patterns are fixed in time, prove phase locking.

As for the relative occurrence of the three stable patterns, a plausibility argument consists in noticing that the extra-ring couplings should make a pattern “more robust.” Thus, considering that the extra-ring couplings for the three patterns are 7, 4, and 4 and they are shared by 4, 4, and 6 families respectively, we attribute to the three patterns frequencies of occurrence proportional to $7/4$, $4/4$, and $4/6$. Once normalized to the total, they provide probabilities close to the experimental values reported above.

It is crucial to note that the geometrical constructions of Fig. 2 match the ring positions insofar as the rings are broadened. The relative broadening $\Delta q/q$ is around 10% at $\varepsilon = 0.2$. As we scan different ε values, we modify the stabilities of the three patterns as well as the relative contributions of the various rings within each pattern.

In order to measure the energy distribution on the various rings, we delimit on the far-field images six concentric shells, the center of each being positioned at

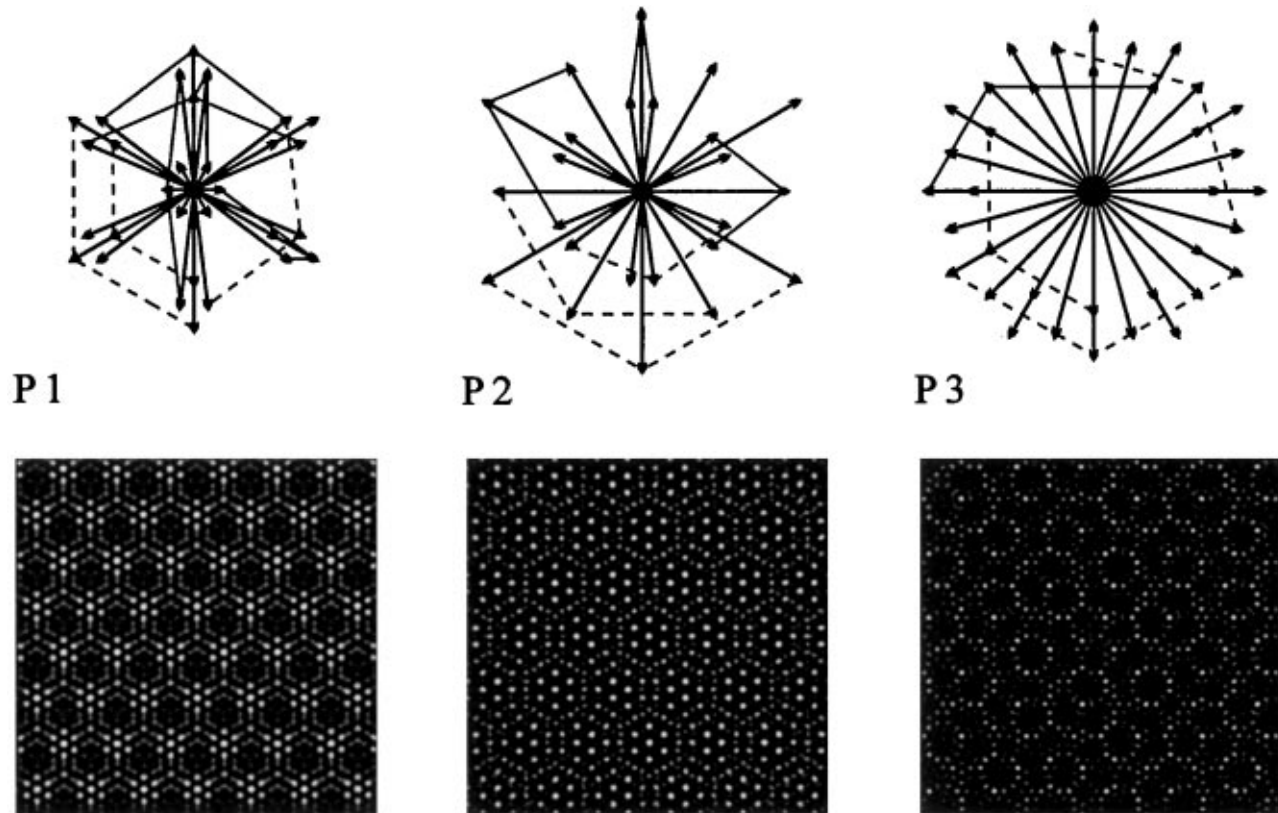


FIG. 2. Upper: wave vector diagrams for P1, P2, and P3. Intraring couplings are indicated by dashed lines and extra-ring couplings by solid lines. Lower: reconstruction of the near field by using the above wave vector summations with the following relative phases (for each excited ring, we indicate the phases in parentheses): P1: 1 (0), 2,2'($\pm\pi/2$), 3 (0); P2: 1,1' (0), 3(0), 5(0); P3: 2,2' ($\pm\pi/2$),3,3'(0),4,4'($\pm\pi/2$).

q_j ($j = 0$ to 5) and measure the power S_j integrated over the j th shell. The measurement is done with a video recorder provided of digital pause. The recorder is computer interfaced, and a frame grabber permits us to acquire sequentially each recorded image. Since for every pattern the transient is of the order of some seconds, we set a time resolution of 0.4 sec by selecting one frame every ten. Then, we extract the intensities S_j connected with each ring j as well as the total intensity $S = \sum_j S_j$.

With reference to 11 equally spaced input intensity values (ϵ from 0.05 to 0.6), we have recorded 30 transient events for each ϵ and isolated those cases relative to pattern P1.

We average over all the recorded transients the stationary value reached by each ring and plot $\langle S_j \rangle$ as a function of ϵ [Fig. 3(a)]. It can be seen that the ring intensities do not grow linearly with ϵ , as it should be expected if there were no wave vector coupling. On the contrary, the stationary value of the averaged total intensity $\langle S \rangle$ over all patterns grows linearly, as shown in Fig. 3(b).

As we switch on and off the intensity, the transient buildup of each pattern takes a time which should depend on ϵ . By averaging over many transients the growth rate of the total intensity S , we evaluate the characteristic

time τ for the buildup of a pattern. The resulting τ is nearly constant and around 7.4 sec (Fig 4). No critical slowing down is observed for small values of ϵ . This time is the same for P1, P2, and P3, even though for P3 the reached plateau does not last forever at high ϵ . Since we know already that the leading nonlinearities in the amplitude equations are the quadratic ones [3] responsible for hexagons formation, we expect normal

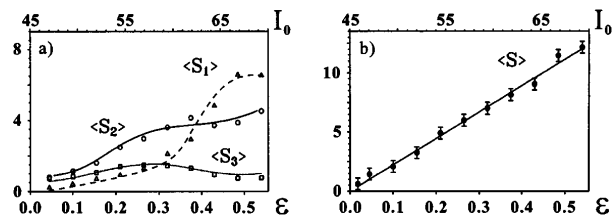


FIG. 3. Stationary values of the intensities (arbitrary units) as a function of the input intensity I_0 ($\mu\text{W}/\text{cm}^2$) or of the normalized control parameter ϵ . (a) $\langle S_1 \rangle$ (triangles), $\langle S_2 \rangle$ (circles), and $\langle S_3 \rangle$ (squares) averaged over P1 patterns; (b) total intensity $\langle S \rangle$ averaged over all patterns. In (a) the lines are guides for the eyes, whereas in (b) the solid line is a linear best fit of the experimental data in order to localize the threshold value $I_{th} = 45.3 \mu\text{W}/\text{cm}^2$.

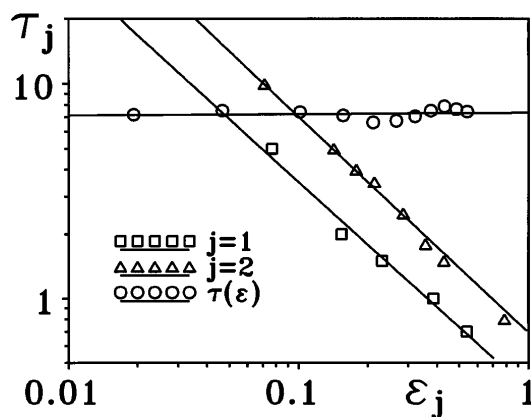


FIG. 4. Buildup time τ (circles) for a phase-locked pattern as a function of the pump parameter ε . The best fit with a power law provides $\tau \approx 7.36\varepsilon^{-0.007}$; i.e., no critical slowing down is observed in presence of ring-ring coupling. We report also the individual ring buildup times τ_j as a function of their respective pump parameter ε_j for $j = 1$ (squares) and $j = 2$ (triangles). The solid lines are best fits with a power law $\tau_1 \approx 0.37\varepsilon_1^{-0.98}$ and $\tau_2 \approx 0.69\varepsilon_2^{-1.00}$.

form equations which provide transcritical bifurcations [11]. This should be the case for a single ring decoupled from the other ones, in which case we have a uniform texture of hexagons.

In order to verify such a fact, we insert in the feedback loop a band-pass filter allowing only one ring. In this condition and for different values of the input intensity I_0 , we register 10 transients for ring $j = 1$ and 2 separately, and evaluate the buildup times τ_1 and τ_2 of the intensity S_1 and S_2 , respectively. From the linear fit of $\langle S_1 \rangle$ and $\langle S_2 \rangle$ vs I_0 , we evaluate the individual ring thresholds $I_{th_1} = 47.1 \mu\text{W}/\text{cm}^2$ and $I_{th_2} = 50.7 \mu\text{W}/\text{cm}^2$, respectively. Then, we define the individual pump parameters ε_j , in the same way as ε , with the replacement of I_{th} with the individual ring threshold intensity I_{th_j} . In this case we find that S_j grows with a buildup time τ_j which scales as ε_j^{-1} , as shown in Fig. 4.

Thus, suppressing extra-ring interactions we recover critical slowing down. On the contrary, the presence of extra-ring interactions, which leads to the collective phase-locked behavior, acts as an extra term which destroys the bifurcation, replacing it with a line of stable fixed points [11].

In conclusion, we have reported the formation of a new kind of two-dimensional patterns due to phase locking of the Fourier amplitudes. This process is quite slow and characterized by a buildup time τ that does not depend on the distance from threshold.

After completion of this Letter, a recent paper was brought to our attention [12] dealing theoretically with patterns emerging from two different wavelengths. However, Ref. [12] does not face the phase-locking problem.

This work has been partially supported by the EEC Contract No. CII*CT93-0331.

*ECM Phys. Department, University of Barcelona, Barcelona, Spain.

†Also, Physics Department, University of Florence, Florence, Italy.

- [1] For a review on optical patterns, see F. T. Arecchi, *Physica D* **51**, 450 (1991); F. T. Arecchi, *Physica D* **86**, 297 (1995), and references therein.
- [2] For a review of pattern formation in different fields see, e.g., M. C. Cross and P. C. Hohenberg, *Rev. Mod. Phys.* **65**, 851 (1993).
- [3] W. J. Firth, *J. Mod. Opt.* **37**, 151 (1990).
- [4] E. Pampaloni, S. Residori, and F. T. Arecchi, *Europhys. Lett.* **24**, 647 (1993).
- [5] E. Pampaloni, P. L. Ramazza, S. Residori, and F. T. Arecchi, *Phys. Rev. Lett.* **74**, 258 (1995); H. Muller, *Phys. Rev. E* **49**, 1273 (1994); M. Le Berre *et al.*, *Phys. Rev. A* **54**, 3428 (1996).
- [6] S. Residori, P. L. Ramazza, E. Pampaloni, S. Boccaletti, and F. T. Arecchi, *Phys. Rev. Lett.* **76**, 1063 (1996).
- [7] S. A. Akhmanov, M. A. Vorontsov, V. Yu. Ivanov, A. V. Larichev, and N. I. Zheleznykh, *J. Opt. Soc. Am. B* **9**, 78 (1992).
- [8] P. C. Hohenberg and B. I. Shraiman, *Physica D* **37**, 109 (1989).
- [9] G. D'Alessandro and W. J. Firth, *Phys. Rev. A* **46**, 537 (1992).
- [10] G. D'Alessandro, E. Pampaloni, P. L. Ramazza, S. Residori, and F. T. Arecchi, *Phys. Rev. A* **52**, 4176 (1995).
- [11] S. Wiggins, *Introduction to Applied Nonlinear Dynamical Systems and Chaos* (Springer-Verlag, New York, 1990), Chap. 3.
- [12] E. V. Degtyarev and M. A. Vorontsov, *J. Mod. Opt.* **43**, 93 (1996).